# Ultrafast Solvation Dynamics at Silica/Liquid Interfaces Probed by Time-Resolved Second Harmonic Generation†

**Xiaoming Shang, Alexander V. Benderskii, and Kenneth B. Eisenthal***

*Department of Chemistry, Columbia University, New York, New York 10027*

*Received: February 14, 2001; In Final Form: May 30, 2001*

The static absorption and ultrafast solvation dynamics of a tricarbocyanine dye IR144 at the silica/acetonitrile and the silica/butanol interfaces were investigated by using steady-state second harmonic generation (SHG) spectroscopy and pump−probe time-resolved SHG (TRSHG) experiments. At both interfaces, the peak wavelength for the $S_0 \rightarrow S_1$ transition of adsorbed IR144 is significantly red-shifted with respect to the maximum absorption wavelength in the corresponding bulk solvent. Because IR144 is negatively solvatochromic, this shift is indicative of a smaller polarity at the interface. A theoretical model of TRSHG is discussed which allows extraction of the solvation dynamics correlation function from the time dependence of the TRSHG signal measured in the pump−probe experiment at a chosen probe wavelength. The time constant for the diffusive component of solvation at the silica/acetonitrile interface was found to be $1.05 \pm 0.14$ ps. It is somewhat shorter, although of the same order of magnitude, than the time constant for the diffusive solvation in bulk acetonitrile, 2.23 ps. At the silica/butanol interface, a time constant of $1.20 \pm 0.15$ ps was extracted, whereas in the bulk butanol, the corresponding diffusive solvation is biexponential with times of 3.5 and 33 ps.

## 1. Introduction

Physical and chemical properties of solid/liquid interfaces have been a subject of long-standing interest because of their importance in both fundamental sciences such as electrochemistry,[1] surface science,[2] and biochemistry[3] and practical applications such as solar energy harvesting.[4] Many aspects of the interfacial solvation process, such as equilibrium solvation energies, dynamical time scales, and molecular mechanisms are still unknown, although they are critical to address the fundamental problems including stability of colloids,[5] electron transfer at electrodes,[6] and molecular processes in biological pores and membranes.[3] Although it is one of the important properties of a solid/liquid interface, the solvation dynamics of species within the interfacial region has been paid relatively little attention. Solvation dynamics usually proceed on an ultrafast (subpicosecond to picosecond) time scale,[7−10] and experimental studies with the corresponding temporal resolution are required for the complete characterization of this process. In the past few years, there have been several theoretical simulation studies on the solvation dynamics of dipolar solvents near various kinds of solid surfaces.[11−13] Even fewer experimental studies have been reported,[14] mainly because of a lack of available techniques suitable for studies of solvation dynamics at interfaces. Such techniques must combine surface specificity with a femtosecond time resolution. To investigate solvation dynamics in bulk media, many experimental techniques have been developed such as time-resolved fluorescence Stokes shift (TRFSS),[7−10,15−17] transient absorption,[18] and nonlinear optical spectroscopic techniques including optical Kerr effect,[9,19−21] photon echo peak shift,[18,22−24] and transient grating.[18] Although these methods proved to be very successful in probing the solvation dynamics in the bulk, their application to studies of interfaces is not straightforward because the observed signal would be overwhelmed by the bulk contribution, and so extraction of the interfacial solvation information is difficult. One approach to deal with this difficulty is to turn to the second-order nonlinear optical spectroscopic techniques. All of the nonlinear optical techniques for bulk-phase solvation studies mentioned above can be described in terms of the third-order optical susceptibility, $\chi^{(3)}$, which is the lowest order nonzero nonlinear term in isotropic bulk media, where second-order ($\chi^{(2)}$) optical nonlinear processes are forbidden in the electric dipole approximation. However, the $\chi^{(2)}$ processes are necessarily allowed at surfaces or interfaces where the inversion symmetry is broken, and this makes the second harmonic generation (SHG) a surface specific technique.[25−27] SHG has been demonstrated to be a unique technique to investigate the absorption properties of probe molecules adsorbed at an interface.[28] Time-resolved second harmonic generation (TRSHG) has been applied to characterize various dynamical processes at interfaces.[2,29,30] Recently, femtosecond laser pulses in a pump−probe setup were utilized to study ultrafast solvation dynamics at the air/water[31,32] and organic surfactant/water interface.[33]

TRSHG is a form of pump−probe spectroscopy where solute molecules are first resonantly excited by an optical pump pulse and then monitored by detecting SHG generated from a time-delayed optical probe pulse.[31] Although the pump may excite solute beyond the interface, the technique only monitors the interfacial solutes due to the surface selectivity of SHG. As a result of resonant pumping, the dipole moment of the probe molecule changes accompanying the ground ($S_0$) to excited ($S_1$) state electronic transition. Because the excitation is sudden, a nonequilibrium interfacial solvent configuration is induced; that is, the solvent structure corresponding to the ground-state solute now surrounds the excited-state molecule which has a different dipole moment. The subsequent relaxation of such a nonequilibrium configuration lowers the free energy of the $S_1$ state.

† Part of the special issue "Howard Reiss Festschrift".

* To whom correspondence should be addressed.

10.1021/jp0105746 CCC: $20.00 
Published on Web 07/19/2001

**SCHEME 1**

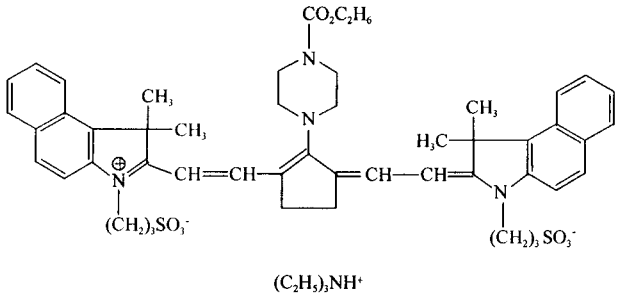

This is the so-called solvation process. Being a spectroscopic technique, SHG is sensitive to this energy relaxation associated with the solvation of the electronically excited state.[31]

Silica was chosen to serve as the solid phase of the solid/liquid interface because of its numerous practical applications, e.g., in various biochemical techniques, and the importance of the physical and chemical properties of the silica/liquid interfaces such as adsorption, adhesions, and catalytic properties.[5] Two solvents, acetonitrile and butanol, were used as liquid phases to form silica/liquid interfaces. Acetonitrile was chosen because it represents a typical polar aprotic solvent, whose solvation dynamics has been well characterized both experimentally[8,15,17,23] and theoretically.[34−37] This allows for a direct comparison of solvation dynamics at the silica/acetonitrile interface obtained in this study with the results for bulk solvent. The silica/butanol interface was also involved in this study because it may provide some general information about solvation occurring at a protic solvent/silica interface. The probe molecule in this study is a tricarbocyanine IR laser dye, IR144, whose molecular structure is shown in Scheme 1. Unlike other commonly used probes of solvation such as coumarin derivatives, IR144 exhibits a pronounced *negative* solvatochromism, which means that the dipole moment of the excited state is smaller than that of the ground state. The supporting spectroscopic evidence is presented in the Results section. IR144 has been shown to be a good probe of the bulk-phase solvation dynamics[18,22−24,38] and can be extended to studies of interfacial solvation. The $S_0 \rightarrow S_1$ transition of IR144 in bulk solvents lies in the 730−800 nm range, i.e., is covered by the fundamental wavelength of the Ti:Sapphire laser system.

In this paper, we report the combined investigation of both the static spectra and the ultrafast solvation dynamics at two planar solid/liquid interfaces, silica/acetonitrile and silica/butanol. The static spectra at the interfaces are measured using the steady-state SHG spectroscopy, and the TRSHG technique is used for the solvation dynamics measurements. The interfacial polarities for the silica/acetonitrile and silica/butanol interfaces, characterized by the spectral shift of the IR144 probe, are smaller than the polarities of the respective bulk solvents, acetonitrile and butanol. The diffusive components of the solvation dynamics observed in our experiments at the interfaces are somewhat faster than the corresponding solvation components in the bulk solvent. Possible mechanisms and interfacial interactions which may lead to the observed differences between the interfacial and bulk-phase solvation are discussed.

## 2. Experimental Section

The measurements of static SHG spectrum and TRSHG were performed using a Ti:sapphire femtosecond laser (Tsunami 9060, Spectra Physics) pumped by an $Ar^+$ laser (BeamLok 2080, Spectra Physics), which generates 10 nJ, ~100 fs laser pulses with a repetition rate of 82 MHz and is tunable from 770 to 900 nm. In the TRSHG setup, probe pulses were split from the output pulse train of the Ti:sapphire oscillator by a beam splitter, whereas the transmitted pulses served as a pump beam. The time delay of the probe pulse relative to the pump pulse was controlled by a computer-driven translation stage (Unislide, Velmex Inc.). A half-wave plate followed by a polarizer was placed in each of the pump and probe beams for controlling their polarizations. The pump beam polarization was 45°. The pump and probe beams were incident at the silica/liquid interface from the silica side, after propagating through a silica prism. The incidence angle was 70° with respect to the silica/liquid surface normal, so that the total internal reflection (TIR) condition was satisfied for both pump and probe beams. The pump and probe beams are separated in horizontal plane by 5°. Both beams were focused and overlapped at the surface by a 7.5 cm focal length lens. To ensure a spatially uniform pump intensity at the sample, the pump beam size was reduced by a telescope before the focusing lens. The pump beam waist at the sample surface was ~20 $\mu$m, 1.5 times larger than the probe beam size of 30 $\mu$m. The power in the pump beam was 200 mW, whereas the probe beam was 40 mW. Identical dynamics were obtained using 80 mW probe power. A colored long-wave pass glass filter was placed in the probe beam immediately before the sample to block any spurious SH radiation. The second harmonic signal generated by the probe beam at the interface was selected with an aperture placed just after the sample and collimated with another 7.5 cm focal length lens. Selecting different components of the $\chi^{(2)}$ tensor was made possible by an analyzer.[25] A colored short-wave pass glass filter was used to block any remaining fundamental light before the SH signal was focused into a monochromator ($^1/_4$ m Digikrom, CVI). The detection system included a photomultiplier tube (R4220P, Hamamatsu), a photon counter, and a computer. Typically an experimental curve is an average of more than 20 data sets.

The experimental setup for steady-state SHG spectrum measurement involves two parallel beams: one of them was used to generate SHG from the sample silica/solution interface, whereas the other generated a reference SHG signal from a silica/neat solvent interface. Identical optics (including half wave plate, polarizer, lens, and silica prism) and liquid sample containers were placed in each arm. Achromatic 7.5 cm focal length lenses were used to focus each beam onto the surfaces, and two 7.5 cm lenses were used to collimate the SHG from the silica/solution interface (sample beam) and the silica/neat solvent interface (reference beam). The use of a movable mirror allowed detection of the SHG signal from either the reference arm or the sample arm. The SHG spectrum of adsorbed solute molecules was obtained by taking a ratio of the SHG signals from the silica/solution interface and the reference silica/neat solvent interface at each wavelength. The use of the SHG reference is important for obtaining a reliable surface spectrum at silica/liquid interfaces because of the changes in laser intensity, pulse width, and the refractive index of silica as the wavelength is tuned. Either acetonitrile or butanol can be used to form the reference interface, at which the SHG spectral response is flat because they are far off resonance in the wavelength region of 770−900 nm. The total internal reflection condition at the silica/liquid interfaces was satisfied in both static and TRSHG setups.

The sample system in this study consists of IR144 solution in acetonitrile or butanol contained in a Teflon beaker tightly covered with a silica prism, so that the liquid is in contact with the silica surface. Prior to each measurement, both the sample

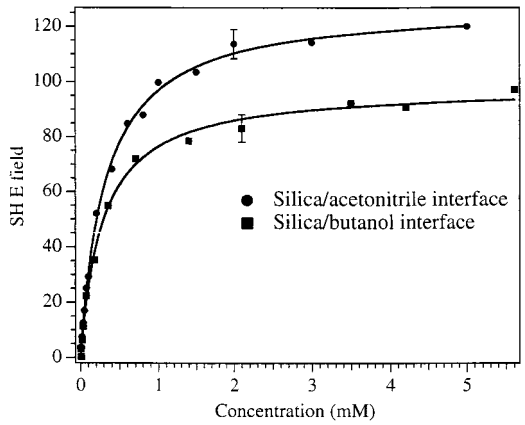


**Figure 1.** Adsorption isotherm of IR144 at silica/acetonitrile (●) and silica/butanol (■) interfaces, measured as the SH electric field as a function of the bulk IR144 concentration. Solid lines show fits to the Langmuir model.

beaker and the silica prism were cleaned by soaking in piranha solution (concentrated $H_2SO_4/H_2O_2 = 2:1$) for 40 min., followed by thorough rinsing with double distilled water, methanol, and then the sample solvent (butanol or acetonitrile). IR144 (Exciton), acetonitrile, and butanol (Aldrich Chemical Co.) were used as received.

Adsorption of IR144 dissolved in the bulk solvents to the silica surface was characterized by recording the resonantly enhanced SH field as a function of the bulk concentration.[39] The resulting Langmuir adsorption isotherms presented in Figure 1 show saturated monolayer formation at bulk IR144 concentrations above ~3 mM. The reported static SH spectra and TRSHG measurements were performed at the bulk IR144 concentration of 35 $\mu$M in both acetonitrile and butanol, which corresponds to $\sim 1/10$ of the saturated monolayer. It was verified that the SH spectra and the solvation dynamics do not change upon increasing the bulk IR144 concentration by a factor of 2.

Orientation of the $S_0 \rightarrow S_1$ transition dipole of IR144 with respect to the interface normal was obtained using the null angle technique[40] modified to take into account the Fresnel factors for the TIR geometry[41] used in our experiment. At both studied interfaces, the transition dipole is nearly perpendicular to the surface. This indicates that the IR144 molecules lie almost "flat" on the surface because the transition dipole is perpendicular to the longest axis of IR144.[42]

To minimize heating and other photon-induced processes in the pump and probe overlap region at the interface, we maintained a low incident laser power and circulated the solution with a stirring bar at ~120 rpm. Under these conditions, no evident sample degradation was observed. The absorption and fluorescence spectra of IR144 in bulk solvents were measured with Perkin-Elmer Lamda 19 spectrometer and Spex Fluorolog F212 fluorescence spectrometer. All experiments were conducted at ambient temperature of approximately 297 K.

## 3. Results

**3.1. Static SHG Spectra.** Steady-state SHG spectra of IR144 at the silica/acetonitrile and silica/butanol interfaces are plotted in Figures 2 and 3, respectively. For IR144 adsorbed at the silica/acetonitrile interface, the SHG spectrum exhibits a single band peaked at ~800 nm, which can be attributed to a one-photon resonance with the $S_0 \rightarrow S_1$ transition. Dashed line shows the fit of the data to a resonant SHG model,[43] briefly described below.

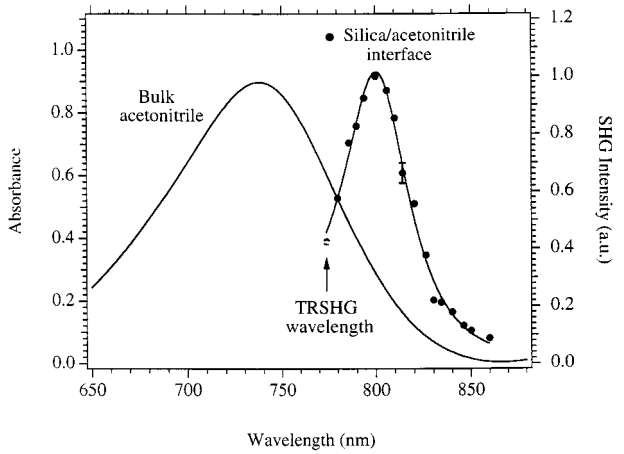


**Figure 2.** Static second-harmonic spectra of IR144 at the silica/acetonitrile interface. The solid circles are the normalized experimental SH intensity versus laser wavelength. The dashed line is the SH spectral fit, described in the text, giving a spectral peak at 803 ± 1 nm. The solid line is the bulk acetonitrile absorbance spectra of IR144 in a 0.5 mm fused silica cell. The bulk absorbance peak is 738 nm. The bulk concentration of IR144 was 35 $\mu$M for both spectra. Arrow shows the probe laser wavelength (774 nm) used in the TRSHG experiments.

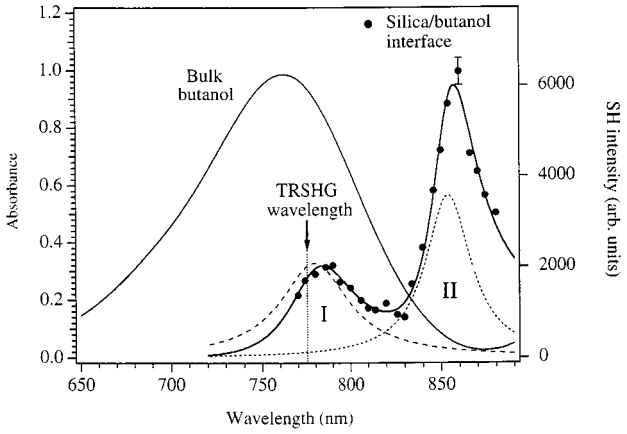


**Figure 3.** Static second-harmonic spectra of IR144 at silica/butanol interface. The solid circles are the normalized experimental SH intensity versus laser wavelength. The two peaks are located at 790 and 860 nm respectively. The solid line is the bulk butanol absorbance spectra of IR144 in a 0.5 mm fused silica cell. The bulk absorbance peak is 762 nm. The bulk concentration of IR144 was 35 $\mu$M for both spectra. Arrow shows the probe laser wavelength (774 nm) used in the TRSHG experiments.

The SHG intensity $I_{SHG}$ is proportional to the squared modulus of the second-order nonlinear susceptibility $\chi^{(2)}$, which includes both the resonant and nonresonant contributions:

$$I_{SHG}(\omega_{pr}) \propto |\chi^{(2)}_{solvent} + \chi^{(2)}_{silica} + \chi^{(2)}_{IR144,NR} + \chi^{(2)}_{IR144,RES}(\omega_{pr})|^2 \quad (1)$$

In eq 1, the terms $\chi^{(2)}_{solvent}$, $\chi^{(2)}_{silica}$, and $\chi^{(2)}_{IR144,NR}$ represent contributions from states far off resonance for neat solvent, silica, and adsorbed solute IR144 and therefore have a weak dependence on the probe frequency $\omega_{pr}$. The term $\chi^{(2)}_{IR144,RES}$ denotes the resonant contribution from IR144. Within the wavelength region of interest (i.e., 770−880 nm), it is likely dominated by a one-photon resonant process which results in the ground state ($S_0$) to first excited state ($S_1$) transition and can be expressed using perturbation theory and a simple two-state model as described in refs 43 and 44. If the three nonresonant terms (i.e., $\chi^{(2)}_{solvent}$, $\chi^{(2)}_{silica}$, and $\chi^{(2)}_{IR144,NR}$) are combined to one term, repre-

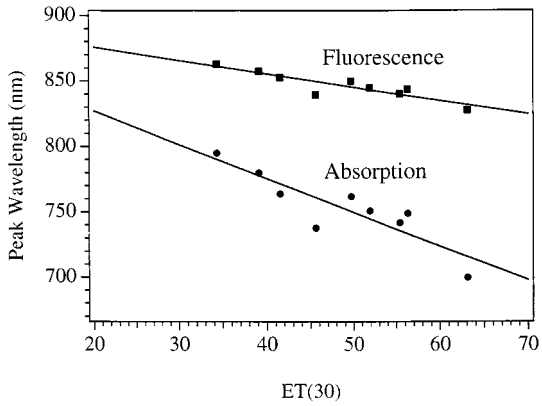


**Figure 4.** Peak wavelength of bulk absorption spectra (●) and peak wavelength of bulk fluorescence spectra (■) of IR144 versus ET(30) of the solvents. The bulk concentration of IR144 was 36 $\mu$M for all of the solution samples. The solid lines are the linear fits.

sented by a constant $B$, eq 1 can be rewritten as

$$I_{SHG}(\omega_{pr}) \propto \left|\frac{A_{ge}}{(\omega_{ge} - \omega_{pr}) + i\Gamma_{ge}} + B\right|^2 \qquad (2)$$

where $\omega_{ge}$ is the center frequency of the $S_0 \rightarrow S_1$ transition, $\Gamma_{ge}$ is its line width, and the factor $A_{ge}$ contains molecular orientation tensor, number of the chromophore molecules, molecular transition matrix elements, and other terms which are weakly dependent on $\omega_{pr}$.

A fit of the static SHG spectrum of IR144 at the silica/acetonitrile interface to eq 2, shown in Figure 2 with a dashed line, gives a spectral peak at $\lambda_{ge}$ ($=1/\omega_{ge}$) of 803 ± 1 nm and a line width $\Gamma_{ge}$ of 330 ± 11 cm$^{-1}$ (fwhm = 42 nm). It should be noted that the center frequency of the $S_0 \rightarrow S_1$ transition $\omega_{ge}$ is about 3 nm to the red of the intensity maximum of SHG spectrum because of constructive interference between the resonant and nonresonant terms in eq 2; that is, constants $A$ and $B$ have the same sign. A similar effect has been previously reported for several interfaces.[32,33,44,45]

For comparison, the linear absorption spectrum of IR144 in bulk acetonitrile is also plotted in Figure 2. It shows that in the bulk solvent the $S_0 \rightarrow S_1$ transition peak is at 738 nm. The observed strong red shift, ~1100 cm$^{-1}$, of the $S_0 \rightarrow S_1$ transition of IR144 at the interface relative to the bulk solvent indicates that IR144 molecules adsorbed at the silica/acetonitrile interface experience a rather different solvation environment (i.e., polarity) than those in the bulk acetonitrile. A measurement of the absorption spectra of IR144 in a series of bulk solvents of different polarities was performed to show that the $S_0 \rightarrow S_1$ absorption peak undergoes a blue shift with increase of the solvent polarity, i.e., IR144 exhibits a negative solvatochromism. Figure 4 demonstrates that the central wavelength (or frequency) is approximately linearly correlated to the ET(30) polarity scale of the solvents.[46] With this result in mind, the red shift of the transition frequency at the silica/acetonitrile interface indicates that the polarity at the silica/acetonitrile interface is smaller than that of bulk acetonitrile.

Assuming that the $S_0 \rightarrow S_1$ transition wavelength for IR144 at the interface follows the same linear correlation with the polarity as that for IR144 in the bulk solvents, one can estimate an ET(30) polarity value of 31 ± 3 for the silica/acetonitrile interface, compared with the ET(30) of 45.6 for the bulk acetonitrile. We must comment, however, on the interfacial polarity in terms of the polarities of the adjacent bulk phases. Although the polarity of weakly interacting gas/liquid or liquid/liquid interfaces is simply an arithmetic average of the two bulk phase polarities,[44] this simple empirical rule cannot be extended to the strongly interacting interfaces such as silica/butanol or silica/acetonitrile. Interactions such as H bonding of the solvent molecules with the silanol groups −SiOH of the silica surface may strongly perturb the local solvent structures at the interface, making the local polarity different from what would be expected based on the polarities of the bulk phases.

Unlike the SHG spectrum of IR144 at the silica/acetonitrile interface, the SHG spectrum of IR144 at the silica/butanol shows two bands (see Figure 3). The SHG spectrum obtained upon diluting bulk solution by a factor of 2 shows the same two peaks with the identical amplitude ratio. Therefore, this bimodal feature cannot be attributed to the aggregates of IR144 at the interface. Although we cannot assign the observed two peaks, the SH spectrum in Figure 3 can be fitted using the same model with two resonant states now, denoted peak I and peak II, which provide coherent (interfering) contributions to the surface $\chi^{(2)}$

$$I_{SHG}(\omega_{pr}) \propto \left|\frac{A_{ge,1}}{(\omega_{ge,1} - \omega_{pr}) + i\Gamma_{ge,1}} + \frac{A_{ge,2}}{(\omega_{ge,2} - \omega_{pr}) + i\Gamma_{ge,2}} + B\right|^2 \qquad (3)$$

The fit is shown with a solid line in Figure 3, and the absolute values of the components peaks I and II are shown in dashed lines. Peak I has center frequency $\lambda_{ge,1} = 1/\omega_{ge,1} = 788$ nm and width $\Gamma_{ge,1} = 24$ nm. Peak II has center frequency $\lambda_{ge,2} = 1/\omega_{ge,2} = 854$ nm and width $\Gamma_{ge,2} = 15$ nm. The amplitude of peak II relative to peak I is $|A_{ge,2}| = 0.83|A_{ge,1}|$. We note that the interference between the two spectral components, which necessarily arises in the coherent SH spectroscopy (all resonantly active species at the interface contribute coherently to the measured SH electric field), results in an apparent shift of the SH peaks relative to the two center frequencies $\omega_{ge,1}$ and $\omega_{ge,2}$, as well as in an apparent amplitude mismatch between the components I and II and the resulting SH spectrum. Both peak I and peak II are well to the red of the absorption peak of IR144 in the bulk butanol. Therefore, even though their assignment is uncertain, we can conclude that the polarity at the silica/butanol interface is less than that in bulk butanol. The use of the ET(30) polarity scale as described above gives an estimate of ET(30) = 36 ± 3 for the silica/butanol interface using the transition wavelength $\lambda_{ge,1} = 788$ nm for peak I and 10 ± 2 for the peak II wavelength $\lambda_{ge,2} = 854$ nm. The bulk butanol ET(30) is 49.7.

A striking difference between the static SHG spectra of adsorbed IR144 at the silica/acetonitrile and silica/butanol interfaces and their respective bulk absorption spectra is that the bandwidths of the SHG spectra (fwhm ~ 700 cm$^{-1}$) are significantly narrower than those of the bulk absorption spectra (fwhm ~ 2000 cm$^{-1}$). Solvatochromic probes have been found to have narrower transition bands relative to bulk values at several other interfaces, including gas/liquid, liquid/liquid, and solid/liquid interfaces[32,33,44]. Thus, it appears that, in general, the interfacial solvation environments tend to exhibit less broadening, perhaps because of less inhomogeneity than the bulk phase.

**3.2. Interfacial Solvation Dynamics.** The temporal SHG signal from IR144 at silica/solution interfaces was measured as a function of the time delay of the probe pulse relative to the pump pulse. Figure 5 shows a typical time dependence of the SH electric field $E_{SH}(t)$, which is defined as the squared root of the SHG intensity, generated at the silica/acetonitrile interface. The $\chi^{(2)}_{zxx}$ element was detected by using $S$ (horizon-

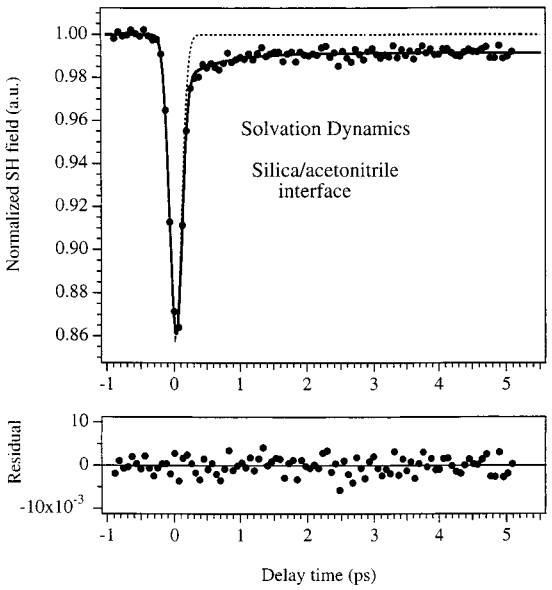


**Figure 5.** Upper panel: Normalized time-dependent second harmonic electric field of IR144 at the silica/acetonitrile interface. The laser wavelength is 774 nm. ZXX element of $\chi^{(2)}$ is detected. Solid circles represent the experimental data. The solid line shows model fit described in the text, giving a time constant of $\tau_S = 1.05 \pm 0.14$ ps. The pump−probe cross correlation function is shown by dashed line at $t = 0$. Lower panel: The residual of the fit.

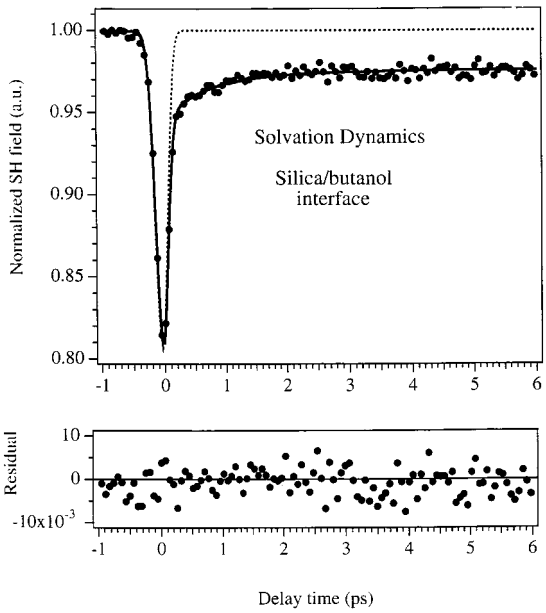


**Figure 6.** Upper panel: Normalized time-dependent second harmonic electric field of IR144 at the silica/butanol interface. The laser wavelength is 774 nm. ZXX element of $\chi^{(2)}$ is detected. Solid circles represent the experimental data. The solid line shows model fit described in the text which gives a time constant of $1.20 \pm 0.12$ ps. The pump−probe cross correlation function is shown by dashed line at $t = 0$. Lower panel: The residual of the fit.

tally) polarized input probe beam and selecting *P* (vertically) polarized output with the analyzer. The probe laser wavelength is 774 nm. Another combination of the polarizer and analyzer, *P* in and *P* out, which primarily detects the $\chi^{(2)}_{zzz}$ element based on the TIR Fresnel factors, gives identical kinetics. As shown in Figure 5, prior to the excitation (i.e., $t < 0$), $E_{SH}$ is constant. Around time zero, $E_{SH}(t)$ is dominated by a sharp spike, which follows the instrument response function shown by the dashed line. Subsequently, a relatively "slow" (ps) exponential recovery is observed. The SH electric field does not go back to the initial baseline within the time window used in this study.

The relative intensity of the spike around time zero depends on the mutual polarization of the pump and probe beams. This feature is in part due to the so-called "coherent artifact", arising because the pump and probe wavelengths in our experiment are the same. However, the spike may include ultrafast dynamics such as intramolecular vibrational relaxation and ultrafast inertial solvation, which cannot be resolved because of the insufficient time resolution in the present experiment. A similar interpretation was proposed to account for the initial spike appearing in the kinetics obtained in transient grating and absorption studies.[18] In particular, we note that, on the basis of the studies in bulk solvents, the vibration relaxation of the probe molecule is usually not observed in the solvation dynamics experiments.[17,23]

After deconvoluting the initial response-limited spike, the general behavior of $E_{SH}(t)$ in a solvation dynamics experiment can be understood as follows. At $t = 0$, one-photon resonant excitation by the pump pulse results in a partial population transfer from the $S_0$ to $S_1$ state of IR144. Both the ground and the excited-state populations of the chromophore contribute to the resonant enhancement of the surface nonlinearity $\chi^{(2)}$. However, within a two-level model, their contributions have opposite phases.[31,47] Therefore, the $S_0$ to $S_1$ population transfer by the pump creates a destructive interference of the optical fields generated by the excited- and ground-state molecules, which accounts for the observed initial bleach of the SH signal. The evolution of the solvation process with time lowers the free energy of the $S_1$ excited state, resulting in the red shift of the "emission frequency" (i.e., transition frequency from $S_1$ to $S_0$). The excited-state thus falls out of the resonance with the probe laser pulse, because the probe wavelength, indicated by arrows in Figures 2 and 3, was chosen to the blue of the transition peak wavelength. This decreases the resonant nonlinearity of the excited-state contribution. As a consequence, a partial recovery of the SH signal is observed, resulting from less cancellation between $\chi^{(2)}$ of the ground state and that of the evolving excited state.

Phenomenologically, the TRSHG data can be fitted to a convolution of the instrument response function with the sum of a single-exponential function which accounts for the slow recovery at $t > 0$, a constant which accounts for the flat background at longer time delay, and a $\delta$ function which accounts for the coherent spike near $t = 0$. The instrument response, i.e., the pump−probe cross-correlation function, was measured by detecting their sum frequency generated at the silica/neat solvent interface in the same experimental geometry. Its fwhm was found to be 240 fs, which reflects broadening of the pulses because of the group velocity dispersion in the silica prism. The fit of the data for the silica/acetonitrile interface gives an exponential decay time of $0.57 \pm 0.07$ ps. The data did not yield a better fit when a biexponential function was used instead of the single exponential. The TRSHG kinetics for silica/butanol interface at a probe laser wavelength of 774 nm is shown in Figure 6. The time dependence was similar to that observed for the silica/acetonitrile interface. Here as well, a single-exponential function with the time constant $0.72 \pm 0.09$ ps reproduces the slow recovery very well.

## 4. Discussion

Solvation dynamics are usually quantified in terms of the solvation correlation function, or the so-called FSS (fluorescence Stokes shift) function,[7,8] defined as

$$S(t) = \frac{\omega_{eg}(t) - \omega_{eg}(\infty)}{\omega_{eg}(0) - \omega_{eg}(\infty)} \quad (4)$$

where $\omega_{eg}(0)$, $\omega_{eg}(\infty)$, and $\omega_{eg}(t)$ are the optical frequencies that correspond to the energy gap between the solvating excited state and the ground immediately after the pump photon is absorbed ($t = 0$), at a time when the solute and solvent have reached equilibrium ($t = \infty$), and at an intermediate time $t$. $S(t)$ is therefore a normalized representation of the solute−solvent interaction energy, as reflected by the $S_1 \rightarrow S_0$ transition frequency of the solvatochromic probe molecule. $S(t)$ changes from 1 to 0 as the solvent reorganizes to reach equilibrium with the solute.

In the bulk-phase TRFSS experiments, $S(t)$ can be measured directly because the experimental observable is simply the excited-state fluorescence, detected as a function of the pump−probe delay. The $\omega_{eg}(t)$ dependence is determined by the so-called spectral reconstruction method[8] from the reconstructed fluorescence spectra at different time delays. In the case of TRSHG, the experimental observable $E_{SH}(t)$ contains coherent contributions from (i.e., interference of) both the excited (time-dependent) and ground (time-independent) states. Below, we briefly outline a procedure for extracting the solvation correlation function $S(t)$ at an interface from the time-resolved SHG measurements of $E_{SH}(t)$. We use the results of the static SHG spectroscopy, which characterizes the time-independent ground-state contribution to the $E_{SH}(t)$, to deconvolute the excited-state dynamics $\omega_{eg}(t)$ from the experimentally measured transient SH signal $E_{SH}(t)$.

A general expression for the time dependence of the second harmonic field measured in a pump−probe TRSHG experiment can be written within the two-level approximation

$$E_{SH}(t) \propto \left| \frac{A_{ge} n_g(t)}{(\omega_{ge} - \omega_{pr}) + i\Gamma_{ge}} + \frac{A_{eg} n_e(t)}{(\omega_{eg}(t) - \omega_{pr}) + i\Gamma_{eg}} + B' \right| \quad (5)$$

where it is assumed that one-photon transitions between only two states, $S_0$ and $S_1$, are in or close to the resonance with the probe frequency $\omega_{pr}$. As in eq 2, all nonresonant contributions are collected in the constant $B'$. The first term on the right-hand side of the equation represents the ground-state contribution (via $S_0 \rightarrow S_1$ "up" transition), whereas the second term represents the time-dependent contribution of the excited state (via $S_1 \rightarrow S_0$ "down" transition) to the nonlinear susceptibility $\chi^{(2)}$. $n_g(t)$ and $n_e(t)$ denote normalized population densities of $S_0$ and $S_1$ states, respectively, $n_g(t) + n_e(t) = 1$. At $t < 0$, i.e., before the pump pulse, $n_g = 1$ and $n_e = 0$, and we recover eq 2 for the static SH signal. Assuming a Gaussian pump pulse of width $\tau_0$, the $S_0 \rightarrow S_1$ transfer rate equation gives

$$n_e(t) = 1 - \exp[-a\{1 + \mathrm{erf}(t/\tau_0)\}] \quad (6)$$

The total transferred population fraction $n_e = 1 - \exp(-2a) \approx 2a$ is determined by the pump pulse energy and the absorption cross-section, and at $t \gg \tau_0$, both $n_e$ and $n_g$ are time-independent. Subsequent evolution of the SH signal therefore is determined solely by the $\omega_{eg}(t)$ in the second term of eq 5. If we assume a single-exponential solvation dynamics correlation function $S(t) = \exp(-t/\tau_S)$, the corresponding $\omega_{eg}(t) = \omega_{eg}(\infty) + [\omega_{eg}(0) - \omega_{eg}(\infty)] \exp(-t/\tau_S)$ can be substituted into eq 5 which is then used to fit the experimental data. A multiexponential function can be used as well to represent the $S(t)$ decay. In the present case, however, this did not result in a better fit of the TRSHG data in Figure 5 within the experimental signal-to-noise.

For the silica/acetonitrile interface, parameters $\omega_{ge}$ and $\Gamma_{ge}$ were obtained by fitting the static SHG spectrum, Figure 2, to the model eq 2. For the more complicated silica/butanol interface spectrum, Figure 3, parameters for peak I, $\omega_{ge,1}$ and $\Gamma_{ge,1}$, obtained from the fit to eq 3 were used because peak II is far off resonance with both the TRSHG probe and pump wavelengths, 774 nm.

The equilibrated excited-state transition frequency $\omega_{eg}(\infty)$ can, in principle, be accurately determined from the steady-state $S_1 \rightarrow S_0$ emission peak frequency.[17] However, determination of the steady state emission spectrum of IR144 adsorbed at the interface presents considerable experimental difficulties because of the large IR144 fluorescent bulk signal. In our analysis, we rely on an estimate of $\omega_{eg}(\infty)$ on the basis of the assumption that the steady state emission spectrum of the solute at the interface is similar to that in the bulk solvent of the same polarity as the interface. The measurements of the steady-state emission spectra of IR144 in a series of bulk solvents of different polarities presented in Figure 4 show that emission peak frequency (or wavelength) is linearly correlated with the ET-(30) of the solvent. Given an ET(30) polarity of 31 for silica/acetonitrile interface determined by the fit of the static SHG spectrum, we find $\omega_{eg}(\infty) = 11\,560\ \mathrm{cm}^{-1}$ (i.e., $\lambda_{eg}(\infty) = 1/\omega_{eg}(\infty) = 865$ nm). Similarly, for peak I at the silica/butanol interface, ET(30) = 36, we estimate $\omega_{eg,1}(\infty) = 11\,670\ \mathrm{cm}^{-1}$ (i.e., $\lambda_{eg,1}(\infty) = 1/\omega_{eg,1}(\infty) = 857$ nm).

Although we can estimate the center wavelength of the $S_1 \rightarrow S_0$ transition from the interfacial polarity considerations, no information can be obtained regarding the line width of this transition, represented by $\Gamma_{eg}$ in eq 4. The bulk-phase TRFSS spectral reconstruction studies show that the line width of the transient emission spectrum of the solute in the bulk is similar to that of the absorption spectrum and does not change notably with the time.[17] It is reasonable to make an assumption that this also holds for the solute at an interface. Accordingly, in the following fit, we simply assume that $\Gamma_{eg}$ is equal to $\Gamma_{ge}$, the latter determined from the static SHG spectra (Figures 2, 3). The finite laser pulse width was incorporated into the fit by a standard convolution of the instrument response function with eq 5.

Figure 5 shows the fit of the data for the silica/acetonitrile interface using a single exponential $S(t)$ function. The solvation dynamics time constant was determined to be $\tau_S = 1.05 \pm 0.14$ ps. The TRSHG results obtained at the silica/butanol interface are shown in Figure 6 together with the fit to the model of eq 5. The solvation time scale extracted for the silica/butanol interface is $\tau_S = 1.20 \pm 0.15$ ps.

The phenomenological fit of the TRSHG data described in the Results section give the time constants of 0.57 ps for the silica/acetonitrile and 0.72 ps for the silica/butanol interfaces, which are similar, although somewhat shorter, than the extracted $\tau_S$. Directly fitting the $E_{SH}(t)$ data obtained at a chosen probe wavelength is similar in spirit to the so-called linear wavelength method devised for the bulk-phase solvation dynamics measurements.[7,15,48] The idea is to find a probe wavelength at which the solvation dynamics correlation function $S(t)$ is directly proportional to the experimental observable, i.e., fluorescence intensity in the case of the bulk-phase TRFSS or $E_{SH}(t)$ in the case of the surface TRSHG. Using the model described above, TRSHG transients can be simulated for different probe frequencies $\omega_{pr}$.

The simulations show that when the probe frequency is on the blue side of the $\omega_{ge}$, the SH signal shows a monotonic

recovery with a time constant similar to the solvation dynamics correlation function time $\tau_S$. This was the situation in our measurements using the 774 nm probe, indicated by arrows in Figures 2 and 3. The fitting shows that for this choice of the probe wavelength the choice of $\Gamma_{eg}$ and $\omega_{eg}(\infty)$ does not significantly affect the extracted time constant for the solvation dynamics. For example, changing $\Gamma_{eg}$ by 50% results in the extracted $\tau_S$ which is different by less than 20%. If, however, the probe wavelength is close to the peak or on the red side of the static SHG spectrum, the calculations show that a more complicated behavior of $E_{SH}(t)$ is expected, such as nonmonotonic recovery in some particular cases. Such behavior was indeed observed when 820 nm probe wavelength was used. In this case, it is difficult to extract $S(t)$ from $E_{SH}(t)$ because the fitting procedure becomes extremely sensitive to the choice of parameters $\omega_{eg}(\infty)$ and $\Gamma_{eg}$ (vide supra).

Being a prototype of a simple polar aprotic solvent, the solvation dynamics of acetonitrile have been extensively studied both experimentally[8,15,17,23] and theoretically.[34−37] Several probe molecules have been used to measure the solvation dynamics of acetonitrile, including IR144. Because the observed solvation dynamics may be varied with the probe molecule to some extent,[37] we only cite the result for bulk acetonitrile probed with IR144, which is the solute used in this study. Similar to other solvents, two solvation dynamics components were observed in bulk acetonitrile using the three pulse echo peak shift technique.[23] The ultrafast inertial solvation component has a Gaussian temporal profile with a characteristic time of 73 fs and accounts for about 70% of the total solvation energy. The slower diffusive solvation component is exponential with a time constant 2.23 ps. It is associated with large amplitude diffusional motions that involve significant reorganization of the solvation structure.

The limited time resolution of our experimental setup does not allow observation of the ultrafast inertial solvation component at the silica/acetonitrile interface. It is likely buried in the coherent artifact spike on the SH signal around $t = 0$. The observed $\tau_S = 1.05$ ps relaxation most likely represents the diffusive component of the interfacial solvation dynamics. It is interesting to compare the time scales of this relaxation mode in the bulk solvents and at the solid/liquid interfaces. Although they are of the same order of magnitude, the diffusive solvation at the silica/acetonitrile interface appears to be faster than in the bulk acetonitrile. Similar to the silica/acetonitrile interface, the solvation dynamics at the silica/butanol interface, $\tau_S = 1.2$ ps, appears to be of the same order of magnitude yet faster than the bulk-phase butanol relaxation, where two diffusive time scales, 3.5 and 33 ps were measured.[18] Because of the insufficient signal-to-noise, we cannot rule out the existence of a longer (>10 ps) solvation component at the silica/butanol interface. A time-resolved fluorescence study of the solvation dynamics at the sapphire/butanol interface using the total internal reflection (TIR) has been reported.[49] Because of the 60 ps time resolution, only the longest diffusive solvation component, ~170 ps, was observed at the interface, which is slower than the 80 ps time scale for the bulk.

An unambiguous interpretation of the molecular mechanism of solvation at the silica/acetonitrile and silica/butanol interfaces would require a detailed MD simulation involving accurate interaction potentials. Here, we only qualitatively consider the interfacial interactions which may affect the relaxation dynamics of the solvent near the interface, in light of the published theoretical and experimental studies of solid/liquid interfaces. The presence of the silanol groups at the silica interface most likely affects both the arrangement of the solvent molecules in the interfacial region and the orientation of the adsorbed solute molecules. The solvation process involves complex many-body dynamics, i.e., simultaneous motions of many solvent molecules. The modified solvent structure near the interface compared to the bulk may therefore result in different static solvation (polarity) and different dynamical relaxation time scales. The adsorbed IR144 may be hydrogen-bonded with the silanol group of the silica surface. The librational motions involving these hydrogen bonds may serve as an additional (faster) solvation channel to lower the free energy of the nonequilibrium excited state and, therefore, shorten the overall solvation processes at the interface. It must be emphasized that, on the basis of the solvation dynamics studies in bulk solvents, there is no direct relation of lower polarity with faster solvation. The polarity, after all, is a *static* equilibrium property, and its connection with the solvation *dynamics* is not straightforward. The lower polarity/faster solvation correlation found in our work might therefore be fortuitous. For example, bulk water is one of the most polar solvents, whereas its solvation dynamics is the fastest of all liquids studies up to date.[8] For the air/water interface, polarity was found to be approximately half of that of the bulk water, but the solvation dynamics are similar to the bulk water dynamics.[32]

Computer simulations of solvent dynamics at a planar hydrophobic wall[12,13] indicate that the diffusive solvation at that neutral solid/liquid interface can be slower than that in the bulk solvent.[12] The simulated hydrophobic interface is, however, rather different from our hydrophilic silica surface terminated by silanol groups. The differences between the simulation results and our experimental findings point to the importance of the local solvent−surface interactions in determining both the structural and dynamical properties near the interface. The significant dependence of the simulation results on the boundary conditions was indeed noted.[12] Another noteworthy aspect is a fairly large size of the polyatomic solute IR144 used in this study. In contrast, a diatomic solute was used in the simulation, which may not represent well the IR144 molecule. The bulk-phase solvation dynamics are to a certain extent dependent on the properties of the solute used such as size, polarizability, etc..[37] Therefore, the use of a more realistic solute seems necessary for obtaining more accurate simulation results.

A similar effect was recently observed in TRFSS experiments at the interface of water/$ZrO_2$ nanoparticles, where the overall solvation time was found to be faster than that in the bulk water.[14] Several mechanisms were proposed to explain the faster solvation dynamics at this interface, including the disruption of the hydrogen bond network of the solvent (water) near the interface because of the formation of hydrogen bonds between the interfacial water molecules and surface OH groups. The net result is the reduction of the H-bond order for the water molecules near the interface, which are thus allowed to move more freely than in the bulk. Related to that is a recent work of our group, which demonstrated the overall reduction of the solvation response time by the hydrophilic surfactant at the air/water interface.[33] There as well, the rearrangement of the hydrogen-bonding network of water molecules near the interface by interactions with the hydrophilic carboxyl group of the stearic acid surfactant was suggested to facilitate the diffusive relaxation of the water molecules.

## 5. Conclusions

Static electronic spectra and subpicosecond solvation dynamics of a molecular probe IR144 at the silica/acetonitrile and silica/butanol interfaces were measured to characterize solvation

at these interfaces. Both the static solvation (polarity) and the dynamical relaxation time scales were found to be different from the corresponding properties of bulk solvents. The central wavelength for $S_0 \rightarrow S_1$ transition of IR144 adsorbed at silica/acetonitrile interface is 803 nm, red-shifted by $\sim$1100 $cm^{-1}$ relative to that in the bulk solution spectrum. Considering the negative solvatochromism of IR144, this indicates that the interfacial polarity is smaller than the polarity of the bulk acetonitrile solvent. A single-exponential relaxation with the time constant of $\tau_S = 1.05 \pm 0.14$ ps was extracted from the pump−probe measurements of the interfacial solvation dynamics. It is assigned to the diffusive solvation component at the silica/acetonitrile interface and is of the same order of magnitude, although somewhat shorter, than the diffusive solvation in the bulk acetonitrile solution, 2.23 ps. The static SHG spectrum for IR144 at the silica/butanol interface exhibits two peaks at 788 and 854 nm, both of which are red-shifted from the bulk transition wavelength. The time-resolved measurements yield the solvation dynamics, $\tau_S = 1.20 \pm 0.15$ ps, for the silica/butanol interface, whereas the corresponding diffusive relaxation components in the bulk butanol are 3.5 and 33 ps. Both the decreased polarity and faster diffusive solvation observed at the silica/acetonitrile and silica/butanol interfaces may be attributed to interactions of the solvent molecules with the silanol groups of the silica surface, which make the interfacial solvation environment different from the bulk phase, both statically and dynamically.

**Acknowledgment.** The authors gratefully acknowledge the National Science Foundation and the Division of Chemical Science, Office of Basic Energy Sciences, of the Department of Energy for their support.

## References and Notes

(1) Weaver, M. J. *J. Phys. Chem.* **1996**, *100*, 13079.
(2) Corn, R. M.; Higgins, D. A. *Chem. Rev.* **1994**, *94*, 107.
(3) Nandi, N.; Bhattacharyya, K.; Bagchi, B. *Chem. Rev.* **2000**, *100*, 2013.
(4) Hagfeldt, A.; Gratzel, M. *Chem. Rev.* **1995**, *95*, 49.
(5) *The Colloid Chemistry of Silica*; Bergna, H. E., Ed.; Advances in Chemistry Series Vol. 234; American Chemical Society: Washington, D.C., 1994.
(6) *Electron Transfer − From Isolated Molecules to Biomolecules*, Part 1 and 2; Jortner, J., Bixon, M., Eds.; Advances in Chemical Physics, Vols. 106 and 107; J. Wiley: New York, 1999.
(7) Barbara, P. F.; Jarzeba, W. *Adv. Photochem.* **1990**, *15*, 1.
(8) Maroncelli, M. *J. Mol. Liq.* **1993**, *57*, 1.
(9) Castner, E. W.; Maroncelli, M. *J. Mol. Liq.* **1998**, *77*, 1.
(10) Jimenez, R.; Fleming, G. R.; Kumar, P. V.; Maroncelli, M. *Nature* **1994**, *369*, 471.
(11) Benjamin, I. *Chem. Rev.* **1996**, *96*, 1449.
(12) Senapati, S.; Chandra, A. *Chem. Phys.* **1998**, *231*, 65; **1999**, *242*, 353.
(13) Senapati, S.; Chandra, A. *J. Chem. Phys.* **1999**, *111*, 1223; **2000**, *113*, 377; **2000**, *113*, 8817.
(14) Pant, D.; Levinger, N. E. *Chem. Phys. Lett.* **1998**, *292*, 200; *J. Phys. Chem. B* **1999**, *103*, 7846.
(15) Nagarajan, V.; Brealey, A. N.; Kang, T. J.; Barbara, P. F. *J. Chem. Phys.* **1987**, *86*, 3183. Kahlow, M. A.; Kang, T. J.; Barbara, P. F. *J. Chem. Phys.* **1988**, *88*, 2372. Kahlow, M. A.; Jarzeba, W.; Kang, T. J.; Barbara, P. F. *J. Chem. Phys.* **1989**, *90*, 151.
(16) Rosenthal, S. J.; Xie, X.; Du, M.; Fleming, G. R. *J. Chem. Phys.* **1991**, *95*, 4715.
(17) Horng, M. L.; Gardecki, A.; Papazyan, A.; Maroncelli, M. *J. Phys. Chem.* **1995**, *99*, 17311.
(18) Joo, T. H.; Jia, Y. W.; Yu, J. Y.; Lang, M. J.; Fleming, G. R. *J. Chem. Phys.* **1996**, *104*, 6089.
(19) Cho, M.; Rosenthal, S. J.; Scherer, N. F.; Ziegler, L. D.; Fleming, G. R. *J. Chem. Phys.* **1992**, *96*, 5033.
(20) Maroncelli, M.; Kumar, V. P.; Papazyan, A. *J. Phys. Chem.* **1993**, *97*, 13.
(21) Chang, Y. J.; Castner, E. W. *J. Chem. Phys.* **1993**, *99*, 113.
(22) Fleming, G. R.; Cho, M. *Annu. Rev. Phys. Chem.* **1996**, *47*, 109. Xu, Q. H.; Scholes, G. D.; Yang, M.; Fleming, G. R. *J. Phys. Chem.* **1999**, *103*, 10348.
(23) Passino, S. A.; Nagasawa, Y.; Joo, T.; Fleming, G. R. *J. Phys. Chem.* **1997**, *101*, 725. Passino, S. A.; Nagasawa, Y.; Fleming, G. R. *J. Chem. Phys.* **1997**, *107*, 6094.
(24) Cho, M.; Yu, J. Y.; Joo, T.; Nagasawa, Y.; Passino, S. A.; Fleming, G. R. *J. Phys. Chem.* **1996**, *100*, 11944.
(25) Heinz, T. F. In *Nonlinear Surface Electromagnetic Phenomena*; Ponath, I., Stegeman, G., Eds.; Elsevier: Amsterdam, 1991.
(26) Shen, Y. R. *Surf. Sci.* **1994**, *299/300*, 551.
(27) Eisenthal, K. B. *Annu. Rev. Phys. Chem.* **1992**, *43*, 627.
(28) Reider, G. A.; Heinz, T. F. In *Photonic Probes of Surfaces*; Halevi, P., Ed.; Elsevier: Amsterdam, 1995; Chapter 9.
(29) Meech, S. R.; Yoshihara, K. *Chem. Phys. Lett.* **1989**, *154*, 20; **1990**, *174*, 423.
(30) Eisenthal, K. B. *J. Phys. Chem.* **1996**, *100*, 12997.
(31) Zimdars, D.; Dadap, J. I.; Eisenthal, K. B.; Heinz, T. F. *Chem. Phys. Lett.* **1999**, *301*, 112.
(32) Zimdars, D.; Eisenthal, K. B. *J. Phys. Chem. A* **1999**, *103*, 10567; *J. Phys. Chem. B* **2001**, *105*, 3993.
(33) Benderskii, A. V.; Eisenthal, K. B. *J. Phys. Chem. B* **2000**, *104*, 11723.
(34) Raineri, F. O.; Resat, H.; Perng, B. C.; Hirata, F.; Friedman, H. L. *J. Chem. Phys.* **1994**, *100*, 1477.
(35) Ladanyi, B. M.; Stratt, R. M. *J. Phys. Chem.* **1995**, *99*, 2502.
(36) Maroncelli, M. *J. Chem. Phys.* **1991**, *94*, 2084.
(37) Kumar, P. V.; Maroncelli, M. *J. Chem. Phys.* **1995**, *103*, 3038.
(38) Hybl, J. D.; Gallagher Faeder, S. M.; Albrecht, A. W.; Tolbert, C. A.; Green, D. C.; Jonas, D. M. *J. Lumin.* **2000**, *87−89*, 126.
(39) Wang, H.; Yan, E. C. Y.; Liu, Y.; Eisenthal, K. B. *J. Phys. Chem. B* **1998**, *102*, 4446.
(40) Heinz, T. F.; Tom, H. W. K.; Shen, Y. R. *Phys. Rev. A* **1983**, *28*, 1883.
(41) Felderhof, B. U.; Bratz, A.; Marowsky, G.; Roders, O.; Sieverdes, F. *J. Opt. Soc. Am.* **1993**, *10*, 1824.
(42) Jonas, D. M. Private communication.
(43) Shen, Y. R. *Annu. Rev. Phys. Chem.* **1989**, *40*, 327.
(44) Wang, H.; Borguet, E.; Eisenthal, K. B. *J. Phys. Chem. A* **1997**, *101*, 713; *J. Phys. Chem. B* **1998**, *102*, 4927.
(45) Yam, R.; Berkovic, G. *Langmuir* **1993**, *9*, 2109.
(46) Reichardt, C. *Chem. Rev.* **1994**, *94*, 2319.
(47) Shen, Y. R. *The Principles of Nonlinear Optics*; Wiley-Interscience: New York, 1984.
(48) Gardecki, J. A.; Maroncelli, M. *J. Phys. Chem. A* **1999**, *103*, 1187.
(49) Yanagimachi, M.; Tamai, N.; Masuhara, H. *Chem. Phys. Lett.* **1992**, *200*, 469.